Lateral forces during atomic force microscopy of graphite in air

David R. Baselt and John D. Baldeschwieler
A. A. Noyes Laboratory of Chemical Physics, California Institute of Technology 127-72, Pasadena, California 91125

(Received 4 February 1992; accepted 7 July 1992)

Highly oriented pyrolytic graphite and boronated pyrolytic graphite were imaged in air by simultaneous normal and lateral force microscopy. A number of effects occurred when scanning over steps, including an increase in attractive forces from surface contamination which could be detrimental to the imaging of soft or weakly bonded samples. Contamination may also give rise to regions of high lateral force which do not seem to be associated with any topographic features. Finally, in atomic resolution images of graphite, atomic corrugation was clearer in the lateral cantilever deflection images than in the simultaneous topography and normal cantilever deflection images, demonstrating the high sensitivity of lateral force detection to topographic features.

I. INTRODUCTION

While normal forces in atomic force microscopy (AFM) have been extensively analyzed both theoretically[1] and experimentally,[2] lateral forces have received less attention.[3] In fact, some of the most interesting results concerning atomic-scale friction have come not from AFM but from van Alsten's modified surface forces apparatus.[4]

Lateral force measurements in combination with AFM provide the opportunity to improve our experimental understanding of the forces acting on the tip and sample during repulsive mode scanning. Lateral force microscopy, also known as frictional force microscopy, was first performed without concurrent normal force detection by Mate *et al.*[5,6] and later by Kaneko *et al.*[7,8] Somewhat later, various schemes were used to acquire lateral force and topography images simultaneously.[9–13]

This article describes results obtained with simultaneous normal and lateral force microscopy on graphite. These results demonstrate that lateral force detection can provide useful information about the tip–sample interaction unavailable from normal force detection alone.

First, however, we wish to clarify two important concepts: the relationship of cantilever deflection to the force exerted on the sample, and the meaning of normal deflection images taken in "constant normal deflection" mode.

Contact force, the repulsive force between the tip and sample at the point where they touch, is currently one of the primary factors limiting image quality. Its measurement is therefore important to AFM. Contact force is generally measured by assuming that it is proportional to deflection ("deflection" will always refer to cantilever deflection in this article). However, this method can produce erroneous results, since a number of forces, most importantly the meniscus force, affect the contact force without affecting deflection.

Both Weisenhorn *et al.* and Burnham *et al.* have described the strong meniscus force which arises, when imaging in air, from the thin film of water vapor and other contamination adsorbed on the tip and sample.[2] The meniscus force acts on the body of the tip and, discounting small sample elasticity effects, does not affect the deflection of a stationary cantilever.

For example, take the case of a cantilever with zero deflection touching a sample in the absence of a meniscus. The contact force is zero. Now allow a meniscus to form, exerting a 10^{-7} N force which pulls the tip and sample together. The contact force increases to 10^{-7} N to balance the meniscus force, but deflection remains unchanged. If deflection were used as a measure of contact force it would, in this typical case, yield a figure that is much too low.

The magnitude of the contact force is equal to the sum of cantilever deflection force (deflection times spring constant) and meniscus force. Therefore, measuring contact force requires knowledge of both deflection and meniscus force. Although meniscus force is usually accounted for by measuring it at one point in an image and then subtracting it out, if it varies within the image, deflection will not be an accurate indicator of contact force. Care must therefore be taken when interpreting deflection images.

Several normal deflection images are presented here which were taken in constant normal deflection mode (usually called "constant force" mode). Following is an explanation of this apparant contradiction. When scanning in constant normal deflection mode, a feedback loop[14] monitors the normal deflection and tries to keep it constant by adjusting "Z" (the separation between the sample and the cantilever base). A normal deflection image is obtained by recording deflection, and a topography image by recording Z. It might be thought that a normal deflection image would therefore be featureless. However, without fluctuations in normal deflection the feedback loop will not change Z, so if the normal deflection image is featureless, the topography will be too. Faster feedback response and slower scan rates reduce the fluctuations in normal deflection, but they never completely disappear.

Since the feedback loop algorithm generates Z by (among other elements[14]) integrating the normal deflection over time, the normal deflection at any given point in a scan is roughly proportional to the slope of the topography at that point.

II. EXPERIMENTAL

The cantilevers used are from Park Scientific Instruments[15] and have 3 μm pyramidal silicon nitride tips.

 0734-211X/92/052316-07$01.00

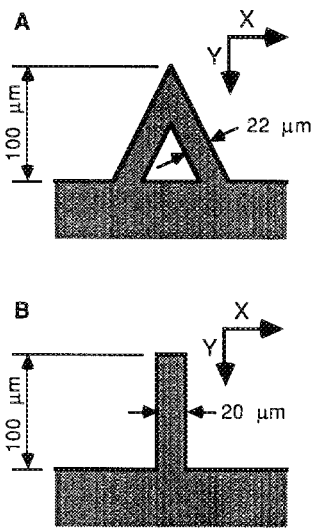

FIG. 1. Diagram of the cantilevers used. The X and Y vectors are the directions of fast and slow rasters, respectively, for a forward scan. In a reverse scan, the X direction is reversed. (A) V shaped cantilever; (B) I shaped cantilever. Both types consist of 0.6 μm thick silicon oxynitride.

100 μm long "I" and "V" shaped cantilevers as diagrammed in Fig. 1 were used. Normal and lateral deflection were detected by an optical lever with a four-segment photodetector, position sensitive in two dimensions, as described by Meyer and Amer.[10] The AFM stage is of our design and scans the cantilever. This produces a slight curvature in topography images (35 Å over a 1 μm scan, in addition to the curvature caused by the tube ceramic), and a more noticable curvature in lateral deflection images. Our electronics were obtained from Topometrix;[16] however, we have written the control and image display software ourselves.

All images were taken in constant normal deflection mode as described above and contain 250×250 data points. Feedback parameters and scan rates were adjusted such that, if the feedback were turned off, Z increased by 50–100 Å, and the feedback restarted, Z would settle back to its old value in the amount of time it takes to acquire one data point (Fig. 2). This step response optimization is essential if the feedback is to respond to features on the surface with adequate speed and without oscillating. It is especially important to the step shape measurements discussed below.

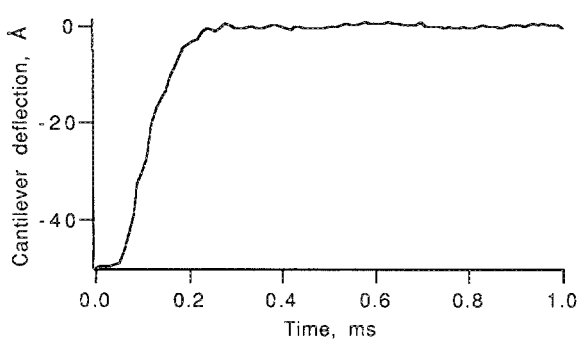

FIG. 2. Typical step response curve. The feedback settles in about 0.25 ms. For most of the images presented in this article, taken at 4 lines/second with 250 points/line in each direction, one data point takes 0.5 ms to acquire. The feedback can therefore respond to most perturbations within one data point.

The images presented are raw data except as described in the figure captions. This paragraph explains the terms used in the captions. In "forward" images, the tip moves from left to right in the figure, while in "reverse" images, the tip moves from right to left. All topography and some lateral deflection images have been "leveled," i.e., the overall tilt, typically 3°–5°, has been removed. Some of the topography and lateral deflection images have been "decurved," meaning that a best-fit paraboloid was subtracted to counter the image curvature described above. Most of the images have undergone postacquisition X hysteresis correction by plotting their data points, not along a regular grid, but in positions determined by a second-degree polynomial. The coefficients of the polynomial were determined by visually matching the position of significant features in the forward and reverse images. All of the forward lateral deflection images were multiplied by -1 so that areas of high friction appear bright in both forward and reverse images.

Up to 10% of the lateral deflection signal appeared as crosstalk in the normal deflection signal, affecting the topography images accordingly. Crosstalk was measured by comparing the difference between the overall height of the forward and reverse topography images (which should be zero) to the difference between the uninverted forward and reverse lateral deflection images (which is always nonzero). Since normal deflection was maintained roughly constant, significant crosstalk did not appear in the lateral deflection images. We did not compensate for crosstalk.

The samples were freshly cleaved *ZYA* grade highly oriented pyrolytic graphite[17] (HOPG) and boronated graphite[18] (BPG). BPG is a form of graphite in which boron atoms substitute for some (about 0.5% in our sample) of the carbon atoms. Since it is of a lower grade than the HOPG, it has more steps and other defects. All samples were grounded to prevent charge buildup.

Normal deflection forces were about 10^{-8} N, exerted downward on the sample. Normal contact forces were about the same as normal meniscus forces, between 10^{-7} and 10^{-8} N. Average normal contact and meniscus forces were determined by taking a force curve upon engaging the sample.[2] Average lateral forces were determined by taking half the average difference between uninverted forward and reverse lateral deflection images: since the average lateral deflection in the reverse scan is the negative of that in the forward scan, the difference between them is twice the average lateral deflection. We use this method so we do not have to measure the lateral deflection zero point. All force measurements rely on calculated values of cantilever spring constants, and are therefore only order of magnitude estimates. We have calculated the lateral spring constant of the wide I cantilevers to be about 53 N/m (including both the torsional and the lateral bending modes) at the tip. By comparing the average lateral deflection signal from I and V cantilevers when scanning the same sample, we estimate

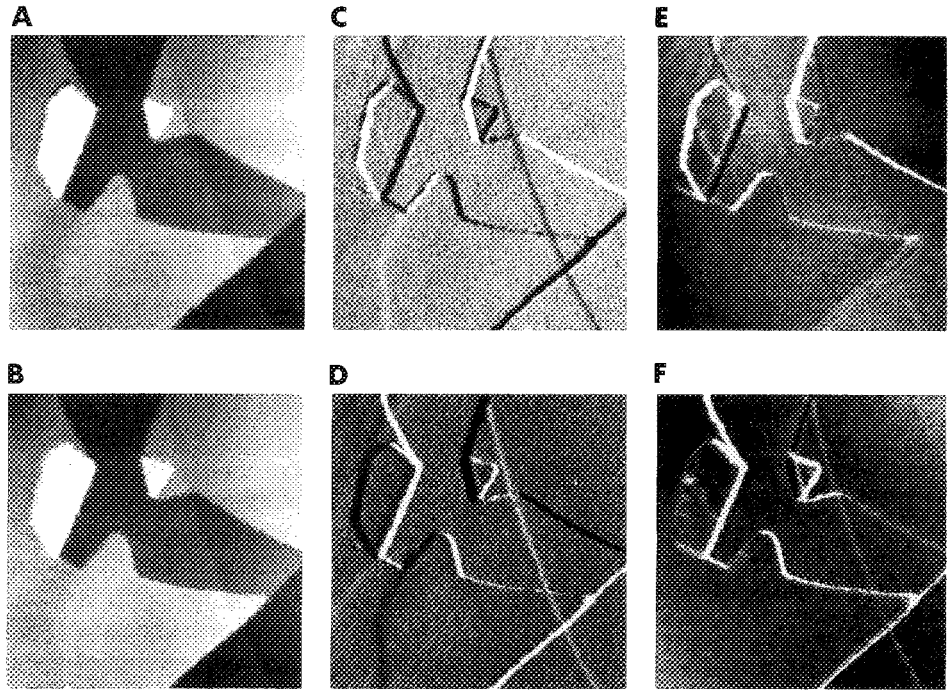

FIG. 3. A 7400 Å scan of BPG. All six images were acquired simultaneously. The diagonal line running vertically through the entire scan is a single atom high step 4 Å tall. The larger steps are 20–50 Å tall. Scan rate 4 lines/second, V cantilever. Corrected for hysteresis. Topography and lateral deflection images leveled and decurved. (A) forward topography; (B) reverse topography; (C) forward normal deflection; (D) reverse normal deflection; (E) forward lateral deflection (multiplied by -1); (F) reverse lateral deflection.

that the lateral spring constant of the 100 μm V is about ten times greater.

III. RESULTS

Figure 3 shows simultaneous topography, normal deflection, and lateral deflection images of an area in which steps 3–50 Å high have been formed when layers of graphite were peeled back while cleaving the sample. A V cantilever was used for this image. The normal meniscus force and the lateral deflection force when scanning over flat areas are both around 5×10^{-8} N. As would be expected, lateral deflection increases when scanning up steps. However, it can be seen that lateral deflection also increases when scanning down steps at a small angle to the scan direction. This effect grows stronger after the graphite has been exposed to air for several hours, so is presumably caused by surface contamination.

Figure 4 shows graphs of topography, normal deflection, and lateral deflection as the tip scans up and down a 50 Å step. The conditions are the same as those for Fig. 3. The scales at the left provide an approximate indication of how large the forces are. Note that the zero points on the topography scales are arbitrary.

A number of features are seen in Fig. 4 and have been numbered, as follows, in order of occurance.

Scanning up a step: (1) Lateral deflection increases before there is any change in normal deflection. (2) Normal deflection increases and the feedback compensates by pulling the cantilever away from the sample, producing the rise in topography. Lateral deflection peaks, and then normal deflection peaks. (3) Near the top of the step there is a shoulder, first in lateral deflection, then in normal deflection. (4) Normal and lateral deflection return to normal as the step comes to an end.

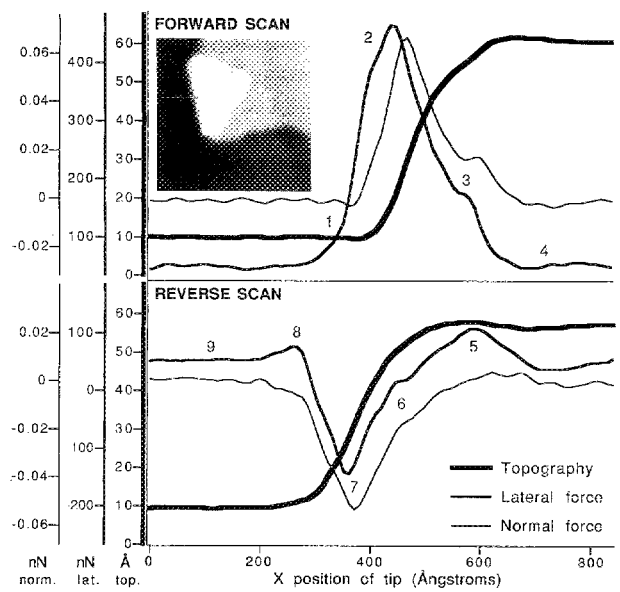

FIG. 4. A 2300 Å forward topography scan of BPG, part of the area shown in Fig. 1, with graphs of topography, normal deflection force and lateral deflection force as the tip scans up and down a 50 Å step. The graphs come from the part of the image marked with a line, and each have 90 data points. Scan rate 4 lines/second, V cantilever. Topography and lateral deflection images leveled; forward normal deflection image multiplied by -1; all images smoothed $3\times$.

Scanning down a step: (5) Lateral deflection increases before the step is encountered. The bright band resulting from this effect in lateral deflection images is sometimes irregular. (6) There is a shoulder in the lateral deflection trace soon after the start of the step. (7) First normal, then lateral deflection goes through a minimum near the bottom of the step. (8) Just after the step ends, lateral deflection increases momentarily. This feature is sometimes absent. (9) Normal and lateral deflection return to normal.

Although some of the above effects (phases 3 and 6 in particular) look as if they might be the result of irregular tip or step shape, all of them have been observed with different tips and samples, on both HOPG and BPG, and on both left-facing and right-facing steps. However, the effects may be more or less pronounced than in Fig. 4. Most notably, the phase 5 lateral deflection increase is often strong enough that there is no drop in lateral deflection when scanning down a step. When this occurs, all steps appear bright in the lateral deflection image.

In addition, the phase 3 peak in lateral deflection is sometimes quite high or broad. Its size has a general correlation with that of phase 5. This is best seen in images taken under water, in which both the phase 3 and phase 5 bands sometimes have the same irregularities. Like phase 5, the height of phase 3 can be great enough to eclipse the "main" peak, sometimes blending into it so only one peak appears. In these cases the only way to identify the type of the peak is from its position relative to the step.

Note that the apparant tip radius in Fig. 4, estimated by dividing the square of the step width by twice the step height, is about 1000 Å. Recall that we have adjusted the feedback parameters and scan rate to insure that our step width measurement is off by no more than one data point (10 Å in Fig. 4). We have measured the radius of two other tips from the same wafer by this method, each on a number of steps 4–50 Å tall, with similar results. This apparant tip radius is much larger than the ~500 Å we expected. The discrepancy could be the result of tip contamination or of step broadening caused by high normal forces (described by Burnham *et al.*).[2] However, it is still possible to take atomic resolution images with these apparently dull tips. We have actually imaged atomic corrugation within the ~100 Å wide area apparently covered by a single-atomic-layer step, a phenomenon which may result when the graphite flexes under the pressure of the tip by more than the height of the step.

In Fig. 5, taken with an I cantilever, there is an area which exhibits high lateral force and is not associated with any topographic feature (the topography image has about 0.5 Å of noise). This area is too broad to be the result of a step. Such sticky areas are quite common, and exhibit 30%–50% more lateral force than the surrounding graphite. They generally have a well-defined polygonal or linear shape.

Figure 6, also taken with an I cantilever, is an atomic resolution image of HOPG. The lateral deflection image strongly resembles one published by Mate *et al.*,[5] although the normal contact force and lateral force in our image are approximately two orders of magnitude smaller. The

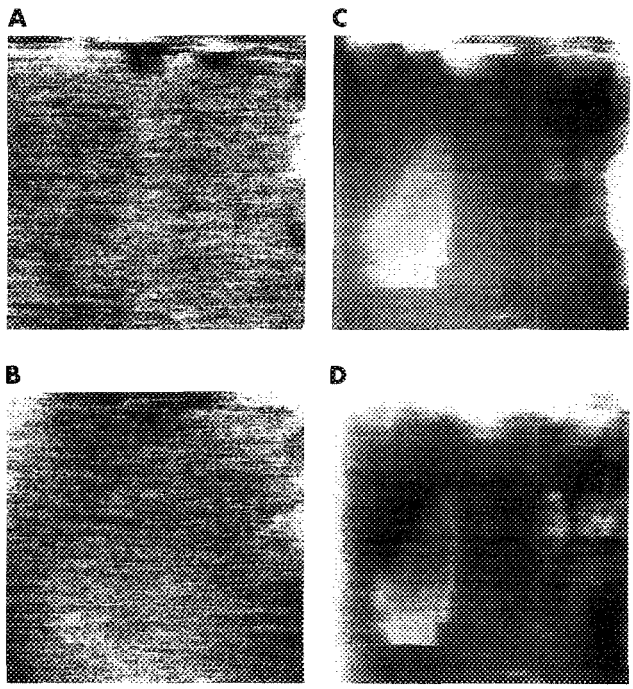

FIG. 5. A 3000 Å scan of HOPG. The lateral deflection images show "sticky spots" not visible in the topography images. Scan rate 4 lines/second, I cantilever. Corrected for hysteresis. Topography images leveled and decurved; lateral deflection images leveled. (A) forward topography; (B) reverse topography; (C) forward lateral deflection (multiplied by −1); (D) reverse lateral deflection.

atomic corrugation is 2.5 Å in topography and 1×10^{-8} N in lateral force. The average lateral force outside smeared regions at the sides of the images is 3×10^{-8} N. The slips in lateral force occur about 1 Å to the right of the peaks in topography in both the forward and reverse scans. This seems to be due to torsional cantilever warpage, since in atomic resolution images taken with V cantilevers the lateral deflection and topography maxima are in the same locations.

With both I and V cantilevers, atomic rows were frequently visible in lateral deflection images but not in normal deflection or topography images. Even when atomic corrugation is discernible in topography and normal deflection images, it is usually clearer in lateral deflection images, as can be seen in Fig. 6. This is presumably a result of the higher optical lever gain of the lateral deflection signal, which has been discussed by Meyer and Amer.[10]

IV. DISCUSSION

Because of the downward force it exerts on the sample, we would expect the tip to resist scanning up a step; i.e., lateral contact force should increase when the tip encounters a step up. Conversely, we would expect lateral contact force to decrease when scanning down a step. A prominent lateral deflection maximum does, in fact, appear when scanning up a step (Fig. 4, phase 2), and a minimum appears when scanning down a step (phase 7), but in addition a number of other features appear.

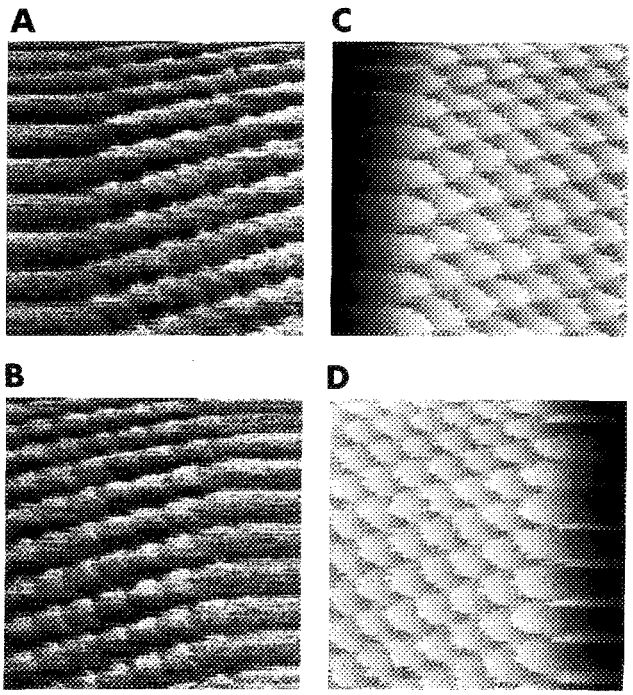

FIG. 6. A 25 Å scan of HOPG. The smearing at the sides of the images is due to the cantilever twisting as lateral force builds up. Similar scans taken with V cantilevers do not show this smearing. Scan rate 10 lines/second, I cantilever. Topography images leveled. (A) Forward topography; (B) reverse topography; (C) forward lateral deflection (multiplied by −1); (D) reverse lateral deflection.

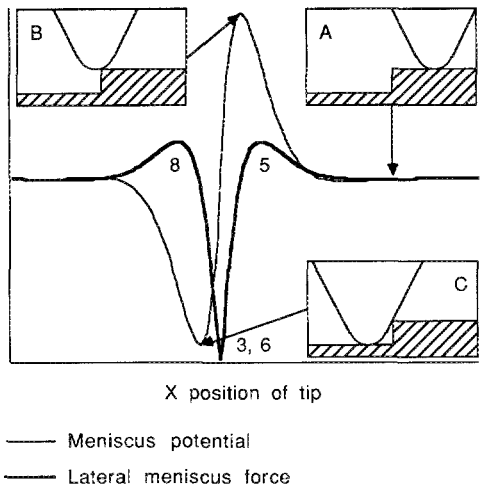

FIG. 7. A hypothesis which describes the observed lateral meniscus forces while scanning down a step. The meniscus itself is not shown. (A) Reference meniscus potential; (B) highest meniscus potential; (C) lowest meniscus potential. The lateral force curve for reverse scans, in bold, is the derivative of the potential taken right to left. For comparison with forward scans, the lateral force curve should be inverted (i.e., the derivative should be taken left to right). Peaks 5 and 8 represent lateral force pulling the tip to the right, peak 3, 6 to the left, regardless of scan direction.

These features, phases 3, 5, 6, and 8 of Fig. 4, are most likely caused by lateral meniscus forces, since they are similar in magnitude (on the order of 10^{-8} N) to the normal meniscus force as measured from force curves. The occasionally irregular shape of phases 3 and 5 and their appearance underwater indicate that insoluble contamination buildup at steps may also be a factor.

The pattern of lateral meniscus forces observed when scanning down a step is consistent with the following hypothesis, illustrated in Fig. 7. Like any other attractive force, the meniscus force can be described by an interaction potential which increases with increasing tip-sample separation. Inset A of Fig. 7 shows the tip before it has encountered the step. In B, the left-hand edge of the tip is further away from the sample, and therefore the meniscus potential is higher than it was in A. Conversely, in C, the right-hand edge of the tip is closer to the sample, so the potential is lower than it was in A. The thin line in Fig. 7 traces out the meniscus potential as a function of the tip position, X. Differentiating this curve with respect to X yields the lateral meniscus force, shown with a bold line. Notice that X increases in the direction of scan, going right-to-left.

Figure 7 indicates that meniscus forces should cause two maxima and one mimimum in lateral force when scanning down a step. This hypothesis therefore explains the high-low-high pattern of lateral deflection when scanning down a step, although the low probably corresponds to the small phase 6 shoulder rather than the larger phase 7 minimum. Phase 7 is probably a result of contact forces, as is suggested by the pattern of lateral forces encountered when scanning up a step.

When scanning up a step, the hypothesized lateral meniscus force curve in Fig. 7 should be multiplied by −1 for comparison with the experimental curve in Fig. 4, which was also inverted. The predicted curve then has a low-high-low pattern, while the experimental curve has a double peak, a high-high pattern. It is likely that the first peak, phase 2, results from contact force, while the second peak, phase 3, results from meniscus force. Our assignment of phase 3 to meniscus force is based on the observation that its height tends to correlate with that of phase 5, which we have already established is due to meniscus force. Based on their positions relative to the step, phase 2 corresponds to phase 7 and phase 3 to phase 6. The two mensicus force minima corresponding to phases 5 and 8 are not visible in the forward scan, probably because they are eclipsed by the phase 2 maximum. These minima are occasionally visible, but we have not been able to image them reproducibly.

Lateral meniscus forces play an important role in AFM imaging and could be a significant factor when trying to image adsorbed molecules (DNA, polymers, proteins) in air. Unlike normal and lateral contact forces, lateral meniscus forces cannot be reduced by pulling up on the cantilever so that it is on the verge of breaking away from the sample.[2] Although they are spread over a wide area and so are not likely to cause much sample distortion, lateral meniscus forces are strong enough that they could pull molecules off the substrate and result in smearing (in contrast to the mechanism which is normally assumed to cause smearing, in which molecules are pushed by contact forces).

In addition, when the tip scans over a step, normal con-

tact force may fluctuate more than the normal deflection image suggests. In Fig. 7(B), the left-hand edge of the tip is further away from the sample than it usually is. Since normal meniscus forces drop off with increasing tip–sample distance, the tip experiences a drop in normal meniscus force. Conversely, in Fig. 7(C) the right-hand edge of the tip is closer to the sample than it usually is, so normal meniscus forces are higher. Since the sum of normal meniscus and contact forces is maintained at roughly zero by the feedback loop, the contact force follows the same trend as the meniscus force. In fact, the normal contact force increases whenever the tip is at the bottom of a valley, and decreases whenever it is on top of a hill.

The fluctuations in normal contact force at steps could become important when imaging, for example, a protein deposited on a flat substrate. Since the protein resembles a step up followed by a step down, the tip will experience fluctuations in contact force when scanning over it. The maximum contact force on a protein could therefore be significantly higher than estimated.

Since, when scanning up a step, lateral deflection appears to increase before normal deflection, lateral deflection might be used as an "early warning" technique. If the lateral deflection signal is multiplied by a constant "k" and is then added into the normal deflection signal, the feedback will respond to steps sooner than it would otherwise, thereby reducing both normal and lateral contact forces on the sample (note that k must be inverted each time the scan changes direction). Incorporating the lateral deflection signal into the feedback loop also helps to compensate for the increased normal meniscus force at steps. The problem with this technique is that, in topography images, it causes sticky or slippery areas to appear higher or lower than they really are.

When analyzing lateral deflection images, it is often helpful to eliminate topographic features so that sticky or slippery areas can be identified. A simple way to do this is to add the forward and reverse lateral deflection images (assuming the forward image has already been multiplied by -1). Since a topographic feature which raises lateral deflection in the forward image will tend to lower it in the reverse image, lateral deflections caused only by topography tend to cancel out. Sticky or slippery areas, though, have the same effect on lateral deflection in both scan directions. These areas double in magnitude and become much more visible. Although the "differential lateral deflection" image is not perfect, because lateral deflection fluctuations over topographic features do not cancel out entirely (Fig. 8), it is still helpful when analyzing complex images.

The exact nature of the observed sticky areas is unknown. On graphite, they often have a well-defined shape, indicating that they may be related to grain structure. Similar sticky areas have been observed on glass with V cantilevers, but they are usually round. We have also seen slippery areas on glass, usually linear or consisting of small spots arranged in strings.

One type of sticky area was expected but never observed. In scanning tunneling microscope (STM) images of BPG, the boron atoms show up as bright spots,[19] and it would be expected that the more reactive boron atoms[20] would likewise produce bright spots in lateral deflection AFM images. However, no evidence was seen of differing lateral force between boron and carbon sites. One possible reason may be that lateral forces in air are so high that the subtle differences, if any, are not observable. Another reason may be that the tip is making contact with the graphite over a large area, so the image represents the average of many atomic interactions rather than just one. Given the large tip radii discussed above, this seems a likely possibility.

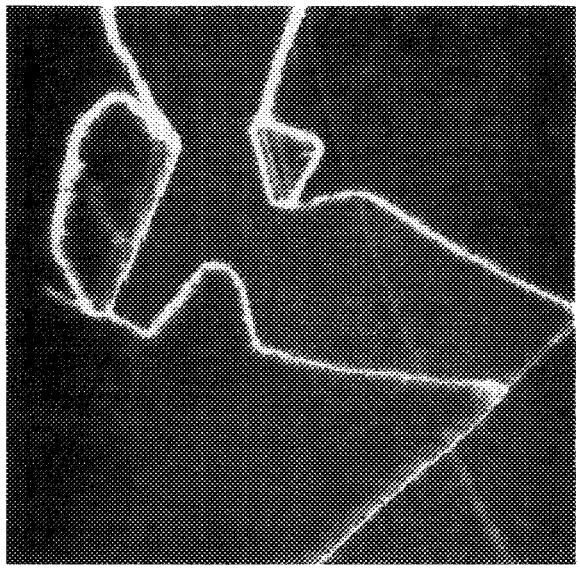

FIG. 8. A differential lateral deflection image generated by adding the forward and reverse lateral deflection images in Fig. 1. Contact forces partially cancel out and all of the steps appear bright due to meniscus force fluctuations.

Finally, it should be noted that I cantilevers provide about ten times more lateral deflection signal than Vs. The additional signal afforded by I cantilevers will become very important when imaging underwater, where lateral forces are greatly reduced. Unfortunately, at the time of this writing I cantilevers are no longer available commercially.

V. CONCLUSION

Lateral deflection measurement can be a valuable analytical tool, providing valuable information about the tip–sample interaction. It is especially worthwhile since the capability is easily added to most optical lever AFMs, and little additional effort is required to record lateral deflection along with topography.

The observations presented in this article indicate that tip–sample interaction forces can be increased by contamination that is not visible in topography images. Perhaps the most ubiquitous example is the rise in meniscus force when steps and valleys are encountered on the sample. Such meniscus force variations cannot be measured with

regular AFM and could be detrimental to the imaging of soft or weakly bound samples.

Lateral deflection sometimes exceeds normal deflection in its sensitivity to topographic features, as evidenced by scans in which atomic corrugation appeared only in lateral deflection images. For some applications, lateral deflection may therefore be the best way to image topography.

Further studies are underway which, in addition to the techniques used in this article, will use both normal and lateral elasticity measurements to measure and perhaps compensate for sample distortion produced by normal and lateral forces.

ACKNOWLEDGMENTS

The authors thank Topometrix for the use of their electronics and A. W. Moore for supplying the boronated graphite. This work was supported by a grant from the Ford Motor Company and a fellowship from the National Science Foundation.

[1]See for example U. Landman and W. D. Luedtke, J. Vac. Sci. Technol. B **9**, 414 (1991); D. Tománek, G. Overney, H. Miyazaki, S. D. Mahanti, and H. J. Güntherodt, Phys. Rev. Lett. **63**, 876 (1989).

[2]A. L. Weisenhorn, P. K. Hansma, T. R. Albrecht, and C. F. Quate, Appl. Phys. Lett. **54**, 2651 (1989); N. A. Burnham, R. J. Colton, and H. M. Pollok, J. Vac. Sci. Technol. A **9**, 2548 (1991).

[3]W. Zhong and D. Tománek, Phys. Rev. Lett. **64**, 3054 (1990); D. Tománek, W. Zhong, and H. Tomas, Europhys. Lett. **15**, 887 (1991); A. J. den Boef, Rev. Sci. Instrum. **62**, 88 (1991), and references 4–13.

[4]See for example J. van Alsten and S. Granick, Tribol. Trans. **33**, 436 (1990).

[5]C. M. Mate, G. M. McClelland, R. Erlandsson, and S. Chiang, Phys. Rev. Lett. **59**, 1942 (1987).

[6]R. Erlandsson, G. Hadziioannou, C. M. Mate, G. M. McClelland, and S. Chiang, J. Chem. Phys. **89**, 5190 (1988).

[7]R. Kaneko, K. Nonaka, and K. Yasuda, J. Vac. Sci. Technol. A **6**, 291 (1988).

[8]R. Kaneko, J. Micros. **152**, 803 (1988).

[9]C. M. Mate, R. Erlandsson, G. M. McClelland, and S. Chiang, J. Vac. Sci. Technol. A **6**, 575 (1991).

[10]G. Meyer and N. M. Amer, Appl. Phys. Lett. **57**, 2089 (1990).

[11]G. Neubauer, S. R. Cohen, and G. M. McClelland, Mater. Res. Soc. Symp. Proc. **153**, 307 (1989).

[12]G. Neubauer, S. R. Cohen, G. M. McClelland, and D. Horne, C. M. Mate, Rev. Sci. Instrum. **61**, 2296 (1990).

[13]S. R. Cohen, G. Neubauer, and G. M. McClelland, J. Vac. Sci. Technol. A **8**, 3449 (1990).

[14]D. R. Baselt, S. M. Clark, M. G. Youngquist, C. F. Spence, and J. D. Baldeschwieler (submitted to Rev. Sci. Instrum). Briefly, our AFM control system uses a digital feedback loop which both reads the normal and lateral deflection and adjusts Z once every 10 μs. For most of the images presented in this paper, one data point corresponds to 50 of these 10 μs feedback cycles. The image data stored for each data point is the average of all 50 readings. The XY raster advances once per feedback cycle rather than once per data point.

[15]Park Scientific Instruments, 476 Ellis St., Mountain View, CA 94043.

[16]Topometrix, 1505 Wyatt Drive, Santa Clara, CA 95054.

[17]Obtained from Union Carbide Coatings Service Corporation, P.O. Box 94924, Cleveland, OH 44101.

[18]Obtained from A. W. Moore, Union Carbide Coatings Service Corporation, 12900 Snow Road, Parma, OH 44130.

[19]R. J. Driscoll, Ph. D. dissertation, California Institute of Technology, 1992.

[20]G. Hennig, J. Chem. Phys. **42**, 1167 (1965).